Properties regulating the nature of the plasmacytoid dendritic cell response to Toll-like receptor 9 activation

Cristiana Guiducci,[1] Gary Ott,[1] Jean H. Chan,[1] Emily Damon,[1] Carlo Calacsan,[1] Tracy Matray,[1] Kyung-Dall Lee,[2] Robert L. Coffman,[1] and Franck J. Barrat[1]

[1]Dynavax Technologies Corporation, Berkeley, CA 94710
[2]Department of Pharmaceutical Sciences, University of Michigan, Ann Arbor, MI 48109

Human plasmacytoid dendritic cells (PDCs) can produce interferon (IFN)-α and/or mature and participate in the adaptive immune response. Three classes of CpG oligonucleotide ligands for Toll-like receptor (TLR)9 can be distinguished by different sequence motifs and different abilities to stimulate IFN-α production and maturation of PDCs. We show that the nature of the PDC response is determined by the higher order structure and endosomal location of the CpG oligonucleotide. Activation of TLR9 by the multimeric CpG-A occurs in transferrin receptor (TfR)-positive endosomes and leads exclusively to IFN-α production, whereas monomeric CpG-B oligonucleotides localize to lysosome-associated membrane protein (LAMP)-1–positive endosomes and promote maturation of PDCs. However, CpG-B, when complexed into microparticles, localizes in TfR-positive endosomes and induces IFN-α from PDCs, whereas monomeric forms of CpG-A localize to LAMP-1–positive endosomes accompanied by the loss of IFN-α production and a gain in PDC maturation activity. CpG-C sequences, which induce both IFN-α and maturation of PDCs, are distributed in both type of endosomes. Encapsulation of CpG-C in liposomes stable above pH 5.75 completely abrogated the IFN-α response while increasing PDC maturation. This establishes that the primary determinant of TLR9 signaling is not valency but endosomal location and demonstrates a strict compartmentalization of the biological response to TLR9 activation in PDCs.

CORRESPONDENCE
Franck J. Barrat:
fbarrat@dvax.com

Abbreviations used: cDC, conventional DC; ISS, immunostimulatory oligonucleotide sequences; LAMP, lysosome-associated membrane protein; ODN, oligodeoxynucleotide; PDC, plasmacytoid DC; ss, single strand; TfR, transferrin receptor; TLR, Toll-like receptor.

Human plasmacytoid DCs (PDCs) represent a central cell type of the immune system (1, 2) that can participate to two of its critical activities. First, they can produce substantial amounts of type I IFN in response to a variety of pathogens, including viruses or parasites (3–6). PDC recognition of viruses is mediated primarily by recognition of the RNA or DNA genomes by Toll-like receptor (TLR)7 and TLR9, respectively (1, 2). Second, after activation by viruses, cytokines, or CD40L, PDCs differentiate into DCs and initiate adaptive immune responses leading to CD4 and CD8 T cell activation (1, 2, 7). The mechanisms governing these two functions, activation of the innate response reflected by IFN-α production and of the adaptive response by increased costimulatory molecule expression and antigen presentation, are not clearly defined. This ability of PDCs to link the innate and adaptive immune response has many potential clinical applications. Clinical trials using synthetic TLR9 ligands, CpG-containing immunostimulatory oligonucleotide sequences (ISS), are currently being conducted in allergy, asthma, cancer, and infectious diseases.

Studies with ISS have revealed an important feature of PDC responses through TLR9. Three different classes of ISS with different primary sequence motifs and different secondary and tertiary structures have been defined. These different classes of ISS produce quite different responses in human PDCs. CpG-A ISS contain poly-G tails that enable the formation of aggregated structures (8) and induce high levels of IFN-α, but have poor activity with respect to inducing the differentiation of PDCs into DCs (9). In contrast, CpG-B ISS induce strong PDC differentiation, but are weak inducers of IFN-α (9). More recently, a third class of ISS, termed CpG-C, has been described that combines high

The online version of this article contains supplemental material.

The Journal of Experimental Medicine

IFN-α induction and efficient maturation of PDCs (10–12). These findings raise intriguing questions concerning the mechanism and biological significance of these different responses of PDCs to TLR9 ligands.

In mice, CpG-A and CpG-B can trigger different signaling pathways involving genes regulated by IRF-7 or NF-κB, respectively (13). This correlates with observations that CpG-A and CpG-B ISS localize to distinct intracellular compartments in mouse bone marrow–cultured DCs (14). In humans, CpG-B have been shown to localize in early endosomes (15); however, these studies were performed with cultured, mature PDCs, which have a much reduced IFN-α production in response to TLR9 (5). The regulation of the IFN-α response can vary dramatically between cell types and culture conditions, stressing the need to study primary cells to characterize the biological responses of human PDCs to TLR9 activation.

The studies reported here were undertaken to better understand the basis for the differential PDC responses to each of the different classes of ISS. We evaluated whether the different biological responses induced by the three classes of ISS resulted from their sequence composition, their secondary/tertiary structures, or their compartmentalization inside the cells. We used several strategies to modify the physical properties of these oligodeoxynucleotides (ODNs) without altering their sequence composition and to correlate their activity on PDCs with ODN structure and localization in endosomal compartments. We also used pH-sensitive liposome preparations to prevent ISS–TLR9 interactions in the specified intracellular compartment to determine whether localization or valency was the primary determinant of the response to TLR9 stimulation. We chose two markers, transferrin receptor (TfR) and lysosome-associated membrane protein (LAMP)-1, to identify endosomal vesicles in PDCs. TfR has been associated in other cell types with early endosomes and/or recycling endosomes and LAMP-1 has been associated with late endosomes and or lysosomes (16, 17). The precise association of TfR and LAMP-1 with specific vesicles has not been clearly defined in primary naive human PDCs; however, it is reasonable to expect these markers to delineate earlier versus later components of the endosome–lysosome pathway. By these means, we were able to define the key factors that control the nature (IFN-α production or differentiation into DC) of human PDCs in response to TLR9 and that provide new insight into the mechanism of action of ISS and a better understanding of the checkpoints regulating PDC activation.

RESULTS

Multimeric display of TLR9 ligands correlates with their ability to induce IFN-α production from human PDCs

Three classes of ISS (CpG-A, -B, -C) with very different biological activities on enriched human PDCs have been described. CpG-A and CpG-C ISS can induce high levels of IFN-α, whereas CpG-B are unable to do so. However, when CpG-B are mixed with PMXB, the ODN is complexed into large microparticles (Fig. 1 B), which transforms it into a potent inducer of IFN-α. The levels of IFN-α induced by CpG-B/PMXB were similar to those induced by CpG-A and CpG-C (Fig. 1 A), whereas PMXB provided relatively little enhancement to IFN-α induction by CpG-A and CpG-C (Fig. 1 A). To determine whether this effect was specific to PMXB formulations, we covalently conjugated CpG-B to the polysaccharide Ficoll to create a large molecule with multiple side chains. CpG-B–Ficoll significantly enhanced IFN-α production by PDCs, although less potently than PMXB formulation (Fig. 1 C). Conversely, when CpG-A was rendered single stranded by heating and flash cooling, a dramatic reduction of IFN-α production was observed (Fig. 1 D). As a confirmation, a stable single- stranded form of CpG-A was

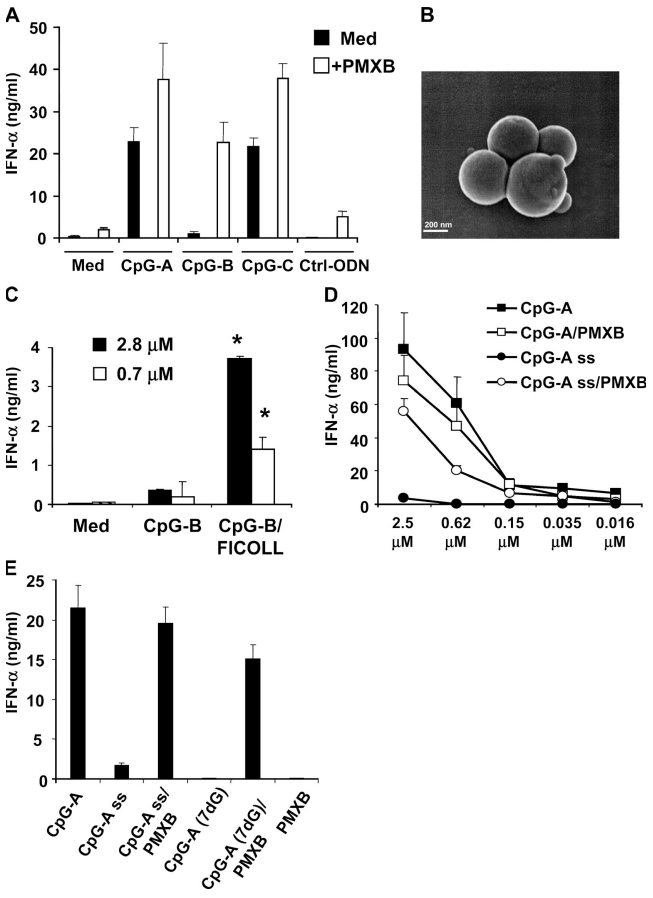

Figure 1. Structural complexity of TLR9 ligands correlates with their ability to induce IFN-α production from PDCs. 5×10^4 purified PDCs were cultured with different concentrations of ISS either alone or in combination with PMXB (100 μg/ml) (A, D, E). (B) Representation of microparticles composed of CpG-B and PMXB using electronic microscopy (Hitachi S-5000). Cells were also stimulated with the indicated concentrations of (C) CpG-B either alone or conjugated with ficoll, (D and E) with the single stranded form of CpG-A (CpG-A ss) and (E) using CpG-A where the last six bases were replaced by 7-deaza-guanosines (CpG-A [7dG]). After 16 h, supernatants were harvested and IFN-α production was evaluated using immunoassay. Averages of 14 (A) and 5 (C–E) independent donors are shown. *, $P < 0.05$.

produced by replacing the poly-G sequence at the 3′ end of the D19 sequence with 7-deazaguanosine residues (CpG-A/7dG). As observed with CpG-A ss, CpG-A/7dG did not induce IFN-α (Fig.1 E). Incorporation of either CpG-A ss or CpG-A/7dG into PMXB microparticles restored them to a multimeric form and restored their ability to induce IFN-α (Fig. 1, D and E). This increase of IFN-α did not result from increased cellular uptake of the ISS (reference 18 and unpublished data). The loss of stimulatory activity of native CpG-A is limited to IFN-α as similar levels of IL-6 are produced after stimulation with CpG-A or CpG-A ss (Fig. S1, available at http://www.jem.org/cgi/content/full/jem.20060401/DC1). These data suggest that the ability of ISS to induce IFN-α is not intrinsic to the sequence composition, but depends upon the ability of ISS to form multimeric structures.

ISS forming highly aggregated structures have decreased capability to induce maturation of human PDCs and subsequent T cell activation

We and others have previously shown that the three classes of ISS have opposite effects on the induction of IFN-α and maturation, with CpG-B being the most potent in inducing PDC maturation. In contrast with their effects on IFN-α production, we observed that CpG-B/PMXB formulations had a reduced activity for PDC maturation as compared with CpG-B alone, both by percentage of cells expressing CD80 and CD86 and by mean fluorescence intensity (Fig. 2, A and B). Conversely, CpG-A are known to be poor inducers of maturation (Fig. 2 C); however, the single-stranded form of CpG-A as well as CpG-A/7dG ODNs induced PDC maturation (Fig. 2, C and D) comparable to that of CpG-B. As with CpG-B (Fig. 2, A and B), the formulation of these two single-stranded ODN with PMXB led to a reduction of maturation activity as compared with free ODN (Fig. 2, C and D). We have shown previously that the level of maturation of PDCs after ISS stimulation can affect their ability to activate naive $CD4^+$ T cells with CpG-B and CpG-C being stronger than CpG-A to promote T cell proliferation (10). Interestingly, when PDC were stimulated with single-stranded CpG-A, they activated T cells as well as PDCs stimulated with either CpG-B and CpG-C (Fig. 3, A and B). Conversely, the incorporation of CpG-B into PMXB microparticles led to a loss of T cell proliferation (Fig. 3, A and B). Altogether, these data strongly suggest that the nature of the biological response of PDCs to ISS largely depends on

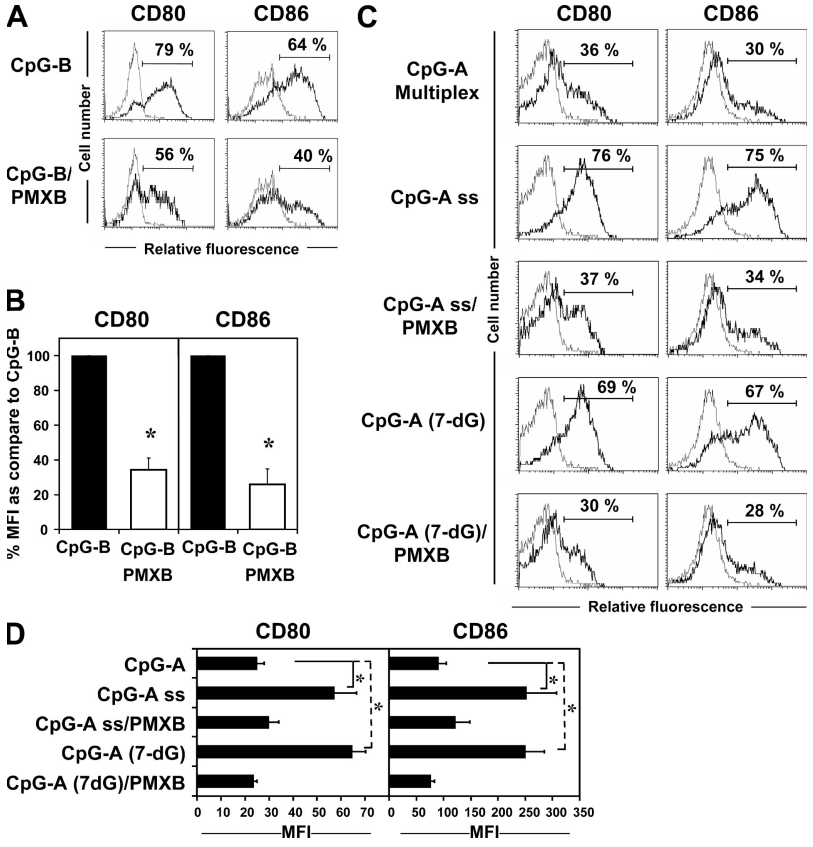

Figure 2. ISS forming highly aggregated structures have decreased capability to induce maturation of human PDCs. Purified PDCs (10^5 cells) were stimulated with ISS (0.1–2 μM) alone or combined with PMXB. After 16 h, cells were characterized for CD80 and CD86 expression by flow cytometry analysis. A and C show representative dot plots, whereas B and D show cumulative mean fluorescence intensities. One representative (A and C) and averages of four independent donors (B and D) are shown. *, $P < 0.05$.

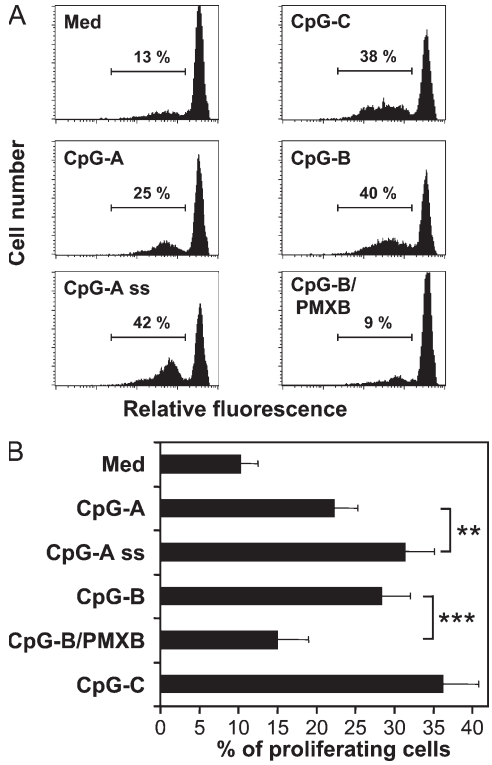

Figure 3. Differential induction of maturation by the different forms of CpG correlates with their ability to promote T cell activation. Purified PDCs (8×10^4 cells) were stimulated with ISS alone or combined with PMXB for 24 h. Naive CFSE-labeled allogenic $CD4^+$ T cells were added (1:2) and incubated for an additional 4 d. Cells were gated on CD3 and examined for the frequency of dividing cells based on CFSE dilution by flow cytometry. (A) One representative and (B) averages of 16 independent MLR reactions are shown. **, $P < 0.01$; ***, $P < 0.001$.

the physical form of the TLR9 ligands, with aggregated structures being able to induce the most potent IFN-α response and single-stranded structures favoring maturation into potent antigen-presenting cells.

The physical form of ISS correlates with their intracellular localization in human PDCs

A recent report demonstrated that the intracellular localization of CpG-A and CpG-B in mouse conventional DCs (cDCs) and PDCs strictly correlated with their ability to induce IFN-α (14). To investigate whether a differential compartmentalization of ISS in human PDCs could account for the aforementioned distinctive biological responses, naive human PDCs were incubated with fluorescent ISS and stained for TfR or LAMP-1 to identify distinct endosomes. Using confocal microscopy, we show that CpG-A were primarily localized in the TfR-positive endosomes, but not the LAMP-1–positive endosomal compartment (Fig. 4, A–D). This was evident even after incubating the cells with fluorescent CpG-A for up to 4 h (unpublished data). CpG- B had a completely different distribution. It was found mainly in the late endosome compartment, as shown by a strong colocalization with

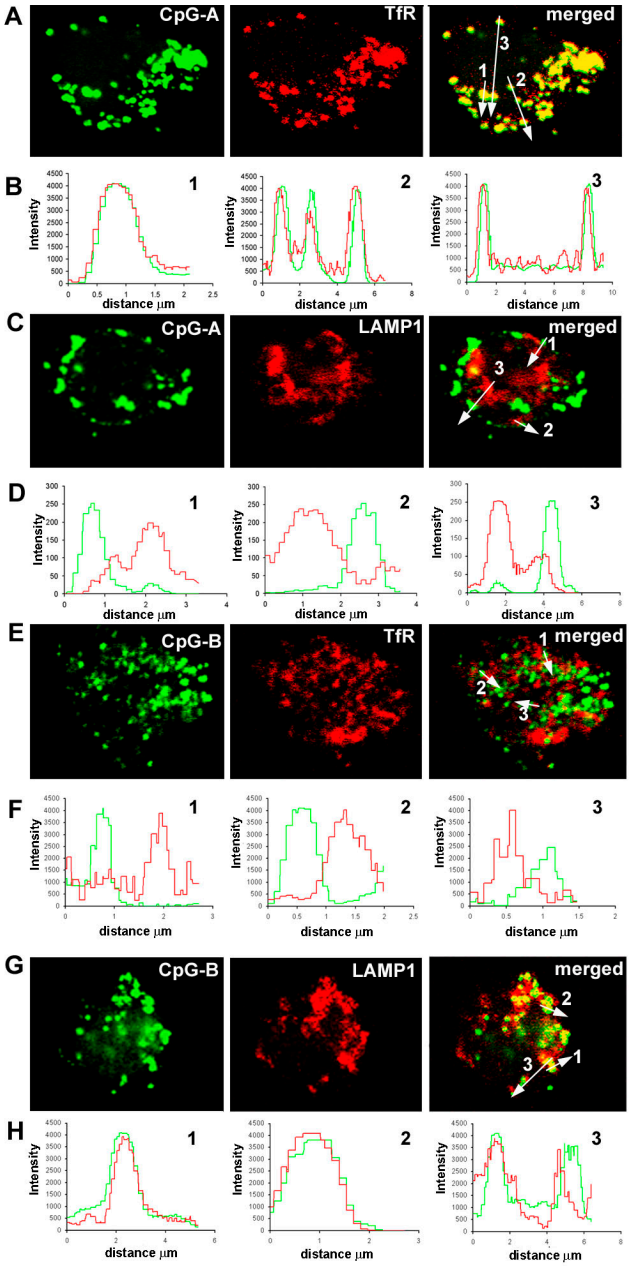

Figure 4. CpG-A and CpG-B are distributed in different compartments in PDCs. Purified PDCs were cultured with fluorescent CpG-A (A and C) or CpG-B (E and G). Cells were fixed, stained intracellularly with (A and E) antitransferrin receptor (TfR) or (C and G) anti–LAMP-1 antibodies, and imaged by confocal microscopy. Images were acquired using a ZEISS LSM 510 META confocal microscope. We used CpG-A-Rhodamine green-X and CpG-B-Alexa488. Intensity profiles of the merged channel along three randomly chosen lines (1, 2, and 3 shown on each merged staining) were analyzed using the profile tools of the Zeiss LSM software. Examples are shown for (B) CpG-A and TfR, (D) CpG-A and LAMP-1, (F) CpG-B and TfR, and (H) CpG-B and LAMP1. The green line represents the intensity of the ISS, whereas the red line represents the intensity of the endosomal marker. Overlap of the two profiles indicates spatial correlation for the occurrence of the two fluorescent signals. Representative data of 5–10 individual donors are shown.

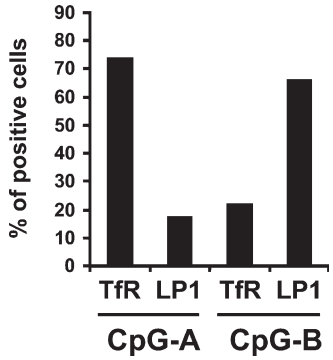

Figure 5. Differential intracellular localization of ISS in human PDCs. Purified PDCs were cultured with fluorescent ISS for 90 min, then fixed and stained intracellularly with antitransferrin receptor (TfR) or anti–LAMP-1 antibodies and imaged by confocal microscopy as described in Fig. 4. Between 25 and 75 cells from at least five different donors were analyzed for colocalization between the ODN and either transferrin receptor (TfR) or LAMP-1 (LP1).

LAMP-1 (Fig. 4, E–H). Interestingly, CpG-C, which has the activities characteristic of both CpG-A (IFN-α induction) and CpG-B (PDC maturation), was found in both the TfR (Fig. S2 A, available at http://www.jem.org/cgi/content/full/jem.20060401/DC1) and LAMP-1 compartments (Fig. S2 C). Human primary PDCs have a small cytoplasm and some degree of colocalization could be the result of overlapping staining patterns. To quantitate the distinction in staining patterns, we analyzed 25–75 cells acquired at high resolution (as in Fig. 4) and showed that CpG-A is colocalized with TfR in 73% of the cells; with LAMP-1, CpG-A is colocalized in only 18% of the cells. Conversely, CpG-B show an opposite pattern (<25% with TfR and 66% with LAMP-1) (Fig. 5). CpG-C was found in both compartments (Fig. S2 E). In addition, using the profile tools of the Zeiss LSM software, we show that the intensity profiles of the merged channels (Fig. 4, A, C, E, and G) along randomly chosen lines reveal a clear spatial correlation for the occurrence of CpG-A and TfR (Fig. 4 B) and for CpG-B and LAMP1 (Fig. 4 H), whereas no correlation was observed between CpG-A and LAMP1 (Fig. 4 D) and CpG-B and TfR (Fig. 4 F). Spatial correlation with both TfR and LAMP-1 was observed when using CpG-C (Fig. S2, B and D). These data demonstrate that the ISS localize in specific organelles in primary human PDCs.

As previously discussed (Figs. 1 and 2), changes in the physical form of CpG-A and CpG-B dramatically altered the biological response of PDCs to these TLR9 ligands. To determine whether these changes correlated with changes in subcellular localization, patterns of fluorescent CpG-A ss and PMXB-complexed CpG-B staining were studied. The single-stranded form of CpG-A, which no longer induced IFN-α but promoted maturation, was observed in the LAMP-1–positive endosomes but not in the TfR-positive endosome compartments (Fig. 6 A). Less than 10% of the cells showed colocalization with TfR, whereas this was observed with

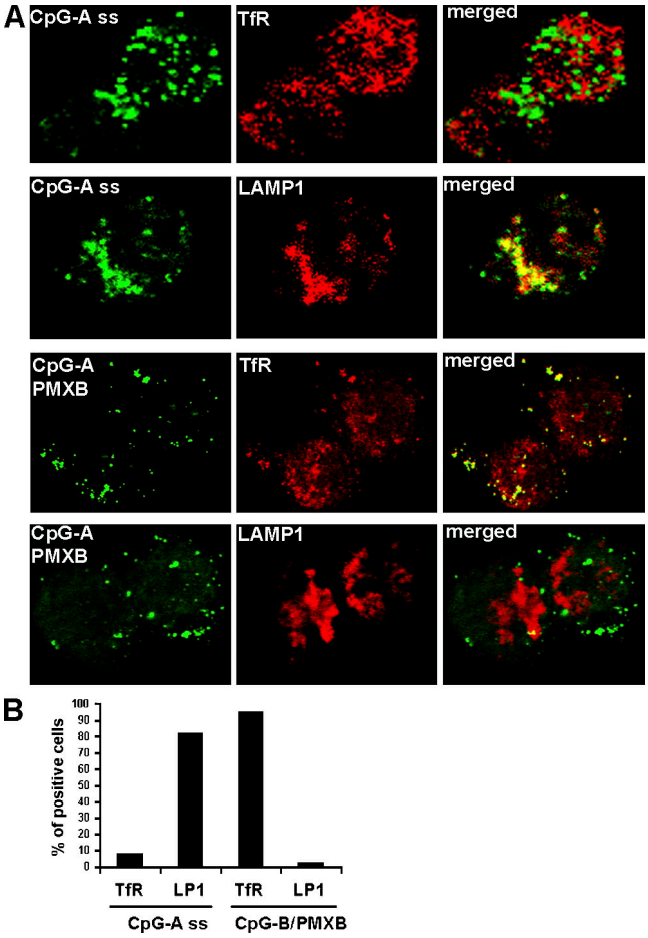

Figure 6. The secondary structure of ISS is regulating their intracellular localization in human PDCs. (A and B) Purified PDCs were cultured with fluorescent ISS for 90 min. Cells were fixed, stained intracellularly with antitransferrin receptor (TfR) or anti-LAMP1 antibodies, and imaged by confocal microscopy. We used CpG-A ss-Rhodamine green-X from the same preparation as CpG-A used in Fig. 4 and CpG-B-Alexa488 premixed with PMXB for 30 min. Images were acquired using a ZEISS LSM 510 META confocal microscope. (B) Between 100 and 200 cells were analyzed from three donors for colocalization between the ODN and either transferrin receptor (TfR) or LAMP-1 (LP1).

LAMP-1 in >80% of the cells (Fig. 6 B). Conversely, CpG-B embedded in PMXB microparticles primarily remained in the early endosomes (Fig. 6 A) with colocalization with TfR in >90% of the cells (Fig. 6 B) and was not found in the LAMP-1–positive endosomes even after 4 h of incubation (Fig. 6 A and not depicted). These data suggest that the same primary sequence can be directed to different intracellular compartments depending on whether it is monomeric or multimeric. Thus, the distinctive functions of each CpG class are not intrinsic to its sequence, but depend on sequence-related second and tertiary structural features. In addition, these data suggest that the nature of the PDC response to TLR9 activation is regulated by the location in which TLR9 and its ligand interact, with induction of IFN-α requiring interaction of the ISS with TLR-9 in TfR-positive endosomes and

PDC maturation requiring ISS interaction with TLR9 in LAMP-1–positive endosomes.

ISS lose their ability to induce IFN-α from human PDCs when encapsulated into pH 5.75 liposomes while they increase their capacity to promote PDC maturation

In experiments shown in Figs. 4–6, there is a consistent correlation between endosomal localization of the ISS and the nature of the PDC response to that ISS. However, the localization of the ISS sequence was varied by changing its physical form, CpG-A, to a single-stranded form and CpG-B by formation of microparticles. It remains possible that monomeric and multimeric ISS deliver different signals through TLR9 regardless of subcellular localization. To test this possibility, we used a CpG-C ISS encapsulated into pH-sensitive liposomes (19) to prevent ISS–TLR9 interaction in vesicles with a luminal pH higher than a specified value. We selected a CpG-C as it can promote both IFN-α and maturation (10) and is naturally found in both early and late endosomes (Fig. S2). Using pH-sensitive liposomes allowed us to control the location of ISS interaction with TLR9, without affecting physical form or valency of the ISS. There is a general agreement that, in many eukaryotic cells, the pH in the early endosomes range between 6.2 and 6.5, in late endosomes between 6.0 and 5.0, and in the lysosomes at a pH <5.0 (20), although no data are available specifically on human PDCs. Based on pH of endosomes and lysosomes in other cell types, we prepared liposomes releasing their content either at a pH <5.0 (Fig. 7 B), so that the CpG-C would be released at a pH found only in lysosomes, or at a pH <6.0 (Fig. 7 C) to prevent interaction between the CpG-C and TLR9 in the early but not in the late endosomes. The pH range over which these liposomes are destabilized is quite narrow as a difference in the 0.25–0.5 pH value is sufficient to permit the complete release of the ODN (Fig. 7, B and C).

We first tested these liposome preparations on B cells to determine whether the encapsulation of CpG-C ISS in liposomes would prevent ISS–TLR9 interaction and therefore activation of the cells. CpG-C ISS encapsulated in liposomes releasing at pH 4.5 had no detectable activity either for cytokine production or induction of maturation, showing clearly that liposomes that remain stable in both early and late endosomes, preventing CpG-C interaction with TLR-9 (Fig. S3, available at http://www.jem.org/cgi/content/full/jem.20060401/DC1). Mixing liposomes with free CpG-C did not impair IL-6 production or B cell maturation, demonstrating that liposomes do not interfere with signaling by ISS that is external to them (Fig. S3). However, CpG-C ISS encapsulated in liposomes releasing at pH 5.75 induced maturation and IL-6 production to a similar extent as CpG-C ISS alone (Fig. S3), showing that release of ISS in the late endosomes permitted complete B cell responses to occur. In addition, we have performed experiments using pH 4.5 liposomes containing both CpG-C ISS and the pore-forming protein listeriolysin (LLO). This will release the ISS in the cytoplasm through pores in the endosomal membrane without prior interaction

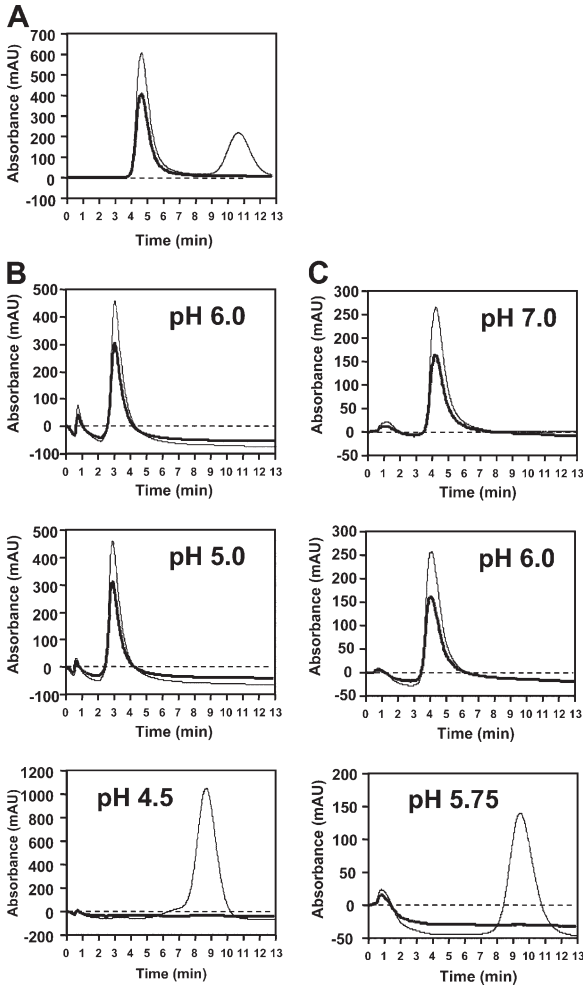

Figure 7. Encapsulation of CpG-C ISS in two pH-sensitive liposome preparations. The liposomes were prepared from mixtures of CHEMS, DOTAP, and PE as described in Materials and methods and purified through gel filtration on a 9-ml Superose 6 column equilibrated with the 0.125 M NaCl, 0.01 M Hepes, pH 8.4 buffer. (A–C) Representation of absorbance monitored at 310 nm (thick line) and 260 nm (thin line) over time is shown. ODN are detected at 260 nm only while the liposomes can be detected at both 260 and 310 nm. (A) Representation of one liposome preparation mixed with free ODN. (B) Representation of one liposome preparation stable until pH < 5.0. (C) Representation of another liposome preparation stable until pH < 6.0.

with TLR9 in endosomes (21, 22). Interestingly, this preparation was also totally inactive (unpublished data), suggesting that the CpG-C needs to enter through the endocytic pathway to have activity. A better definition of the trafficking of these different liposome preparations will be needed in future studies to get a more detailed understanding of their behavior and of their properties once they get inside the cells.

CpG-C ISS can induce both maturation and IFN-α production from PDCs. Strikingly, CpG-C, when encapsulated in pH 5.75 liposomes, could not induce IFN-α from PDCs, as measured either by ELISA or by quantitative PCR (Fig. 8 A and not depicted), although it was even more active at

inducing PDC maturation (Fig. 8, B and C). This demonstrates that CpG-C ISS must interact with TLR9 in vesicles with a pH >6.0 to induce IFN-α, but not maturation. This was specific, as liposomes alone or CpG-C/Lipo 4.5 were totally inactive (Fig. 8). This suggests that the ODN sequence of the different classes of ISS determine their activity indirectly by promoting specific secondary or multimeric structures that control the intracellular localization of the ISS to the appropriate endosomes. However, a single molecular form of CpG-C will stimulate IFN-α only if it encounters TLR-9 in less acidic endosomes, strongly indicating that it is the location of TLR-9 signaling, not valency of the ligand that is directly responsible for the nature of biological response in PDCs.

DISCUSSION

In the present study, we have investigated an important mechanism underlying the diversity of function of human PDCs by analyzing the basis for the different biological responses induced by three distinct classes of synthetic TLR9 ligands. We show that the nature of PDC response to TLR9 activation depends primarily on the intracellular compartment in which the ISS–TLR9 interaction occurs. Whether an ISS is localized to early endosomes, late endosomes, or both is a function of the physical form of the molecule, but is not directly a function of the sequence motifs or backbone chemistry of the molecule. Sequence and backbone are important, however, as both factors influence the equilibrium between simple and higher order structures. Strikingly, the two critical functions of PDCs, IFN-α production and antigen presentation, appear to be regulated by different signaling pathways associated with the different endosomal compartments. Such control is extremely tight as it is possible to uncouple the two responses by properly manipulating the intracellular distribution of the ISS. Thus, when a CpG-B with poor IFN-α induction is embedded in microparticles using PMXB, it becomes an inducer of high levels of IFN-α from PDCs while decreasing the maturation of these cells and their subsequent T cell priming capability, as compared with free CpG-B. Alternately, CpG-A, made single stranded either by sequence modification or heating, lose their ability to stimulate IFN-α production but gain strong maturation induction and T cell priming activity. Interestingly, single-stranded CpG-A embedded in PMXB regains its ability to induce high levels of IFN-α with low levels of PDC maturation. In addition, we show that there is a consistent correlation between the nature of the PDC response to ISS and the intracellular localization where the interaction between ISS and TLR9 primarily occurs. Multimeric structures such as CpG-A or CpG-B/PMXB microparticles are preferentially retained in TfR-positive endosomes of PDCs and this correlates with induction of high IFN-α levels and inefficient stimulation of costimulatory molecule expression. Conversely, single-stranded ODN such as CpG-B or CpG-A ss and CpG-A (7-dG) are strong inducers of maturation but cannot activate PDCs to produce IFN-α and these ODNs are consistently found preferentially in the LAMP-1–positive compartments.

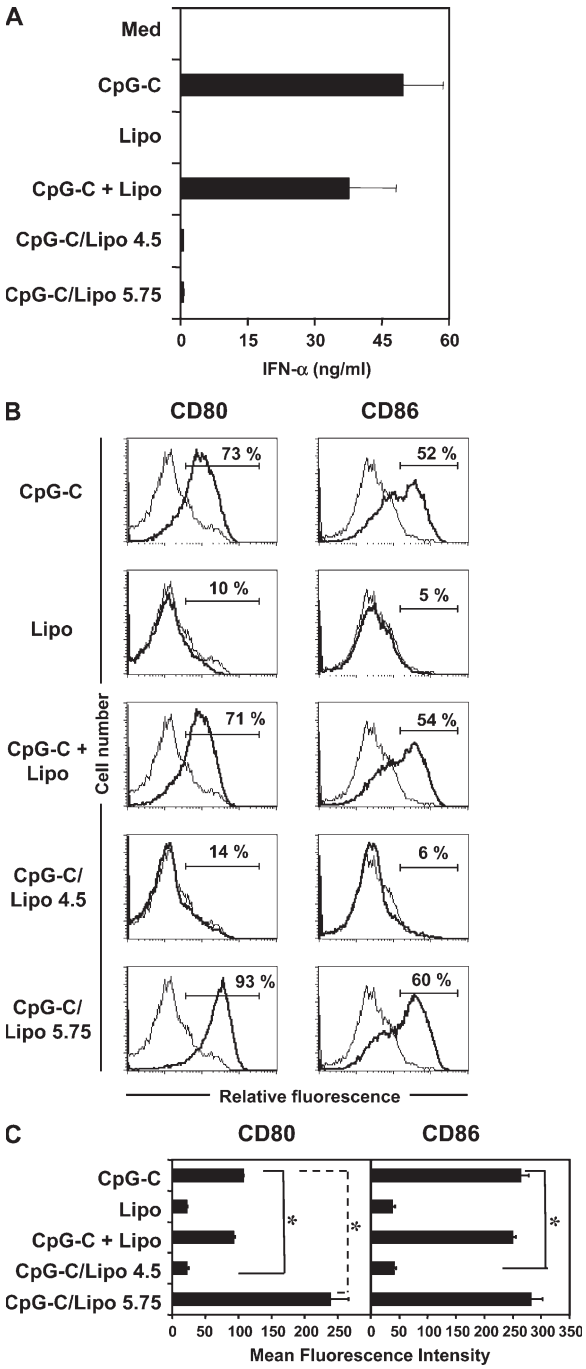

Figure 8. CpG-C ISS lose their ability to induce IFN-α from human PDCs while retaining the ability to induce maturation when encapsulated into pH 5.75 liposomes. Purified PDCs (5×10^4 cells) were cultured with CpG-C (0.5 μg/ml) alone, empty liposomes, CpG-C mixed with empty liposomes, and with CpG-C encapsulated into two different liposome preparations (pH 4.5 or pH 5.75 sensitive) as described in Fig 7. (A) After 16 h, supernatants were harvested, IFN-α production was evaluated using immunoassay, and (B and C) cells were characterized for CD80 and CD86 expression by flow cytometry. (B) Representative dot plots. (C) Averages of the cumulative mean fluorescence intensity for four independent donors representative of 10 donors are shown. *, $P < 0.05$.

The presence of CpG-C in both types of endosomes correlates with their ability to trigger both IFN-α production and PDC maturation. In addition, the fact that CpG-C stimulate both types of PDC response provides evidence that the two signaling pathways are not mutually exclusive. Because of the long palindrome in the sequence, CpG-C can form either hairpin loop structures or can anneal to form dimers, but they do not form larger aggregates, thus they can be considered structurally intermediate between single-stranded CpG-B and multimeric CpG-A (11).

CpG-A form large nanoparticle structures with an average diameter of 50 nm and PMXB forms microparticles ranging from 100 to 500 nm (8, 18). CpG-B conjugated with ficoll has a molecular weight of 500–1,000 kD and an overall size of 20 nm (unpublished data). It is thus possible that TLR9 interaction with multimeric ISS structure would signal only through the IRF7 but not the IRF5–NFκB pathway regardless of the intracellular compartment where the interaction occurs. Alternatively, the intracellular compartment where the different signaling complexes are engaged could be the key factor in triggering a different signaling pathway. Honda et al. have recently shown that to induce IFN-α, mouse cells need to activate the transcription factor IRF-7. Indeed, they show that in RAW 264.7 cells transfected with fluorescent-tagged MyD88 and IRF-7, the two proteins colocalize in early endosome vesicles, suggesting the possibility that the TLR9–MyD88–IRF-7–dependent IFN pathway is started exclusively in the early endosome (14). In mice, although both cDCs and PDCs express TLR9, only the latter are able to produce IFN-α in response to TLR9 ligands with CpG-A being found in the late endosomes in the cDCs. When CpG-A are complexed with DOTAP, they are retained in the early endosome and stimulate cDCs to produce comparable levels of IFN-α to PDCs (14). Thus, the rules governing physical form and endosomal localization appear to be different between cell types and it is important to perform studies in the cell type of interest.

ISS has been suggested to enter the cells via clathrin-mediated endocytosis (15). Contrasting results reported TLR9 to be either localized in the ER in resting cells and then recruited to the site where CpG accumulate (15), or localized in an early endosome (23) together with the Myd88–IRF7 complex (14). Although no data are available on human primary PDCs, it is generally accepted that endocytosed molecules are first delivered to the early endosomes where the sorting process begins. The different endosomal compartments display increasing acidity as they progress in the endocytosis pathways (pH 6.3–6.5 for recycling compartments and pH 5.0–6.0 in late endosomes) and late endosomes can either recycle to the cell surface or proceed to the lysosomal compartment (pH $<$ 5.0) where their content is degraded (20). This acidification can vary between cell subsets and level of activation/maturation of the cells (24).

CpG-C have the unique ability to localize in both early and late endosomes. By encapsulating CpG-C in pH 5.75–sensitive liposomes, we were able to prevent the binding of ISS with TLR9 in the early/recycling endosomes without affecting the physical form of the ODN. In this situation, the CpG-C failed to induce IFN-α from PDCs, but was more potent as an inducer of PDC maturation than CpG-C alone. Interestingly, oligonucleotides released from liposomes only at a more acidic pH (lipo 4.5 preparations) could no longer activate either maturation or IFN-α production in PDCs, suggesting that no significant TLR9 signaling occurs in lysosomal vesicles, in accordance with previous data showing that CpG binding to TLR9 is optimal between pH 6.5 and 5.5 (25). We attempted unsuccessfully to produce liposomes that would be able to release CpG-C at a pH $>$6.2 to evaluate release in the TfR-positive endosomal compartment. The change of composition required to make such liposomes does not allow ODN encapsulation, as their ζ potential is too close to the neutral point.

Previous studies have shown that pH-sensitive liposomes release their contents in vesicles in a pH-dependent fashion (21, 26, 27). It is possible that the actual pH at which each of these liposomes lyses and releases its contents may be altered inside endosomal compartments; however, there is no basis to expect changes in the rank order of lysis of the different liposome preparations. It has been shown that DC maturation is accompanied by a shift in lysosomal pH that becomes more acidic (thereby facilitating protein proteolysis) (24), although the effect of ISS stimulation on this process is currently unknown. As no interaction between ISS and TLR9 is possible before the liposomes actually lyse and release their contents, this is unlikely to affect the release of the initial load of CpG-C.

One question raised by our data is the following: Why are ISS confined to early endosomes only when they are in multimeric form? The mechanisms governing the retention time in the different compartments are still poorly understood. One possibility could be that only small structures are incorporated into multivescicular body inclusions and proceed through the endocytic pathway toward lysosomal compartments, whereas larger structures would not do this and would remain trapped into the early/recycling endosomes (16, 28). Another possibility could be the presence inside the early endosomes of a coreceptor for ISS that would have a higher avidity for large structures and would thereby prevent their transit in the late endosomes. We cannot exclude, however, the possibility that PDCs possess even more specific mechanisms that affect the intracellular trafficking of CpG as suggested by recent studies showing that mouse myeloid DCs, although expressing TLR9, are unable to properly localize CpG-A despite its large structure in the early endosome (14).

Many viruses have evolved to be activated at pH that correspond to early or late endosomes and use various mechanisms to be retained in these endosomes to avoid the destructive effect of lysosome acidification (29, 30). One of the best-described examples is the Semliki forest virus (30–32), entry of which can be prevented by inactivation of Rab5, an essential protein for the function of early endosomes (31, 32). Other

viruses such as influenza will go further down the pathway and reach late endosomes (31). PDCs are unique in their response to viruses, even though other cells, such as cDCs in mice, express TLR7, TLR9, and IRF7 and have the potential to produce similar levels of IFN-α (14). Still, the strikingly different type I IFN response after virus activation of cDCs and PDCs (33, 34) strongly suggests that PDCs are optimized to respond to virus infections. In light of our data and published observations, one model would be that PDCs have adapted to the ability of viruses to stay in endosomes by producing large quantities of the antiviral cytokine IFN-α and, as the virus slowly progresses to late endosomes, maturing into antigen-presenting cells that initiate T cell responses. Thus, the compartmentalization of TLR-9–mediated response may reflect the need of PDCs first to mount an appropriate innate response, but then switch rapidly to function at the interface of the innate and adaptive immune response.

MATERIALS AND METHODS

Oligonucleotide synthesis and formulations. Phosphorothioate ODNs were prepared as described previously (10). The prototypes for the ISS classes used were as follows: CpG-A (D19): 5′-GGtgcatcgatgcagGGGGG-3′; CpG-B (1018 ISS): 5′-TGACTGTGAACGTTCGAGATGA-3′; and CpG-C (C274): 5′-TCGTCGAACGTTCGAGATGAT-3′. Uppercase letters represent PS linkages and lowercase letters represent PO linkages. Single-stranded version of CpG-A (CpG-A ss) was prepared by heating at 95°C for 5 min followed by flash cooling in dry ice for 10 min. CpG-A (7dG) was the same sequence as D19 except that the last six guanosines were substituted with 7-deaza guanosine bases. The resulting ODN is totally single stranded (unpublished data). Inactive control oligonucleotides were selected based on similar lengths with same base composition and no CpG motif and no apparent activity (stimulatory or inhibitory). Fluorescent-labeled CpG ISS were purchased from TriLink BioTechnologies. All ODNs had <5 endotoxin U/mg ODN, determined by *Limulus* amebocyte lysate assay (BioWhittaker). The preparation of 1018-Ficoll400 (CpG-B Ficoll) was similar as described previously (35). In brief, phosphorothioate-linked 5′-1018-$(CH2)_3$SS-$(CH2)_3$OH was reduced with tris (2-carboxyethylphosphine) hydrochloride, purified by RP-HPLC and used immediately in the reaction with aminoethylcarboxymethyl (AECM) 180-Ficoll400, which was prepared by Inman's method (36). On average, there were between 35 and 134 moles of ODN per mole of Ficoll (MW = 400,000 D).

Isolation and stimulation of purified human cell subsets. Buffy coats were obtained from the Stanford Blood Center. All cells were used under Institutional Review Board–approved protocols. PBMCs were isolated as described previously (10). B cells were isolated using CD19 enrichment as described previously (37). Purity was routinely 99%. Experiments were conducted with 2×10^5 B cells per well cultured in 96-flat bottom plates. PDCs were isolated using BDCA-4 enrichment as described previously (37). PDCs were 95–99% $BDCA2^+$ $CD123^+$ as determined by flow cytometry. Experiments were conducted with 5×10^4 PDCs per well cultured in 96-round bottom plates. CpG and PMXB (Sigma-Aldrich; 100 μg/ml) were added separately in the tissue culture medium and let to complex for 30 min at room temperature before being added to the cells as described previously (18).

Cytokines and antibodies. Cytokines levels were measured by ELISA. Human IFN-α and IL-6 production was assayed with reagents from PBL Biomedical Laboratories and CytoSet antibody pairs obtained from BioSource, respectively. Monoclonal antibodies used for flow cytometry included: anti-CD19, anti-CD80, anti-CD86, (BD Biosciences), anti-CD123, and anti–BDCA-2 (Miltenyi Biotec). Monoclonal antibodies used for immunofluorescence analysis were antitransferrin receptor (CD71) and anti–LAMP-1 (CD107a) antibodies and were purchased from BD Biosciences.

CFSE labeling and in vitro naive T cell stimulation. Naive $CD4^+CD45RA^+$ T cells were prepared using a two-step approach using magnetic microbead labeled antibodies (Miltenyi Biotec). First, CD8-, CD11b-, CD16-, CD19-, CD36-, CD45R0-, and CD56-bearing cells were depleted and nondepleted cells were enriched for CD4. Purity was assessed by staining with CD4 and CD45RA antibodies and was routinely ∼99%. Cells were stained with 1 μM CFSE (Invitrogen). For coculture experiments, 8×10^4 PDCs per well were stimulated with ISS for 24 h. CFSE-labeled allogenic naive T cells were added at a ratio of 1:2 (PDC:T cell) in the absence of IL-2. After 4 d, the proliferation of CFSE-labeled $CD4^+$ T cells was measured by flow cytometry.

Preparation of pH-sensitive liposomes. 1,2-dioleoyl-3-trimethylammonium-propane (DOTAP) and L-α-phosphtidylethanolamine (PE) were obtained from Avanti Polar Lipids. Cholesteryl hemisuccinate tri salt (CHEMS) was obtained from Sigma-Aldrich. The pH 5.75 liposomes were prepared from mixtures of CHEMS, DOTAP, and PE (molar ratio 20:10:4), whereas the pH 4.5 liposomes were prepared using CHEMS, PE (molar ratio 45:54). Both preparations were made using the freeze-thawing method based on the procedure of Monnard (38). Lipids were hydrated with 1.0 ml 0.125 M NaCl, 0.01 M Hepes, pH 8.4 buffer containing 20 mg/ml of oligonucleotide and were frozen in liquid nitrogen, then thawed at room temperature five times. Nonencapsulated (free) ODN was removed from the liposome preparation by gel filtration on a 9-ml Superose 6 column (GE Healthcare) equilibrated with the 0.125 M NaCl, 0.01 M Hepes, pH 8.4 buffer. Absorbance was monitored at 260 and 310 nm, and the liposome peak at 310 nm was collected. The liposomes can be detected at both 310 and 260 nm (Fig. 7 A), whereas the ODN are detected only at 260 nm (Fig. 7 A). Liposome mean diameter, size distribution, and ζ potential were determined with a Nicomp 380 ZLS submicron particle sizer. All liposome preparations had mean diameters from 220 to 250 nm and ζ potential (pH = 8.4) between −60 and −68 mV. As the pH decreased, the ζ potential equilibrated until the liposomes destabilized. The concentration of oligonucleotide encapsulated in the liposomes was determined by capillary electrophoresis (CE).

Confocal microscopy. PDCs were incubated with fluorescent-labeled ISS (10 μM) for different time points (45 min, 90 min, and 4 h), washed three times with ice cold PBS, fixed in PBS medium containing 1% paraformaldehyde at room temperature for 15 min, and permeabilized for 10 min with 0.25% saponin 1% BSA in PBS. Samples were blocked for 30 min using Image-iT FX signal enhancer (Invitrogen) and labeled with antitransferrin receptor-PE or anti–LAMP-1–PE in 0.25% saponin 1% BSA in PBS. Images were acquired using a ZEISS LSM 510 META confocal microscope and a 63×/1.4 N.A. objective, with the pinhole set for a section thickness of 0.8 μm (pinhole set to 1 airy unit in each channels). Alexa-488 or rhodamine green-X (green) and PE (red) images were acquired sequentially using separate laser excitation to avoid any cross-talk between the fluorophore signals. Intensity profiles of the merged channel along randomly chosen lines were analyzed using the profile tools of the Zeiss LSM software.

Statistical analysis. Data were analyzed using a two-tailed Student's *t* test. All analyses were performed using Prism software (GraphPad Software). Differences were considered significant at a p-value <0.05.

Online supplemental material. Fig. S1 shows IL-6 production from PDCs in response to multimeric and monomeric forms of CpG-A. Fig. S2 describes CpG-C intracellular localization in PDCs. Fig. S3 depicts B cell response to liposome-encapsulated CpG-C. Online supplemental material is available at http://www.jem.org/cgi/content/full/jem.20060401/DC1.

We would like to thank our colleagues at Dynavax Technologies for their critical reading of the manuscript. We thank H.L. Aaron (U.C. Berkeley) for invaluable assistance with confocal analysis.

This work was supported by the Alliance for Lupus Research.
The authors have no conflicting financial interest.

Submitted: 21 February 2006
Accepted: 29 June 2006

REFERENCES

1. Asselin-Paturel, C., and G. Trinchieri. 2005. Production of type I interferons: plasmacytoid dendritic cells and beyond. *J. Exp. Med.* 202:461–465.
2. Liu, Y.J. 2005. IPC: professional type 1 interferon-producing cells and plasmacytoid dendritic cell precursors. *Annu. Rev. Immunol.* 23:275–306.
3. Svensson, H., B. Cederblad, M. Lindahl, and G. Alm. 1996. Stimulation of natural interferon-α/β-producing cells by *Staphylococcus aureus*. *J. Interferon Cytokine Res.* 16:7–16.
4. Cella, M., D. Jarrossay, F. Facchetti, O. Alebardi, H. Nakajima, A. Lanzavecchia, and M. Colonna. 1999. Plasmacytoid monocytes migrate to inflamed lymph nodes and produce large amounts of type I interferon. *Nat. Med.* 5:919–923.
5. Siegal, F.P., N. Kadowaki, M. Shodell, P.A. Fitzgerald-Bocarsly, K. Shah, S. Ho, S. Antonenko, and Y.J. Liu. 1999. The nature of the principal type 1 interferon-producing cells in human blood. *Science.* 284:1835–1837.
6. Pichyangkul, S., K. Yongvanitchit, U. Kum-arb, H. Hemmi, S. Akira, A.M. Krieg, D.G. Heppner, V.A. Stewart, H. Hasegawa, S. Looareesuwan, et al. 2004. Malaria blood stage parasites activate human plasmacytoid dendritic cells and murine dendritic cells through a Toll-like receptor 9-dependent pathway. *J. Immunol.* 172:4926–4933.
7. Colonna, M., G. Trinchieri, and Y.J. Liu. 2004. Plasmacytoid dendritic cells in immunity. *Nat. Immunol.* 5:1219–1226.
8. Kerkmann, M., L.T. Costa, C. Richter, S. Rothenfusser, J. Battiany, V. Hornung, J. Johnson, S. Englert, T. Ketterer, W. Heckl, et al. 2005. Spontaneous formation of nucleic acid-based nanoparticles is responsible for high interferon-α induction by CpG-A in plasmacytoid dendritic cells. *J. Biol. Chem.* 280:8086–8093.
9. Krieg, A.M. 2002. CpG motifs in bacterial DNA and their immune effects. *Annu. Rev. Immunol.* 20:709–760.
10. Duramad, O., K.L. Fearon, J.H. Chan, H. Kanzler, J.D. Marshall, R.L. Coffman, and F.J. Barrat. 2003. IL-10 regulates plasmacytoid dendritic cell response to CpG-containing immunostimulatory sequences. *Blood.* 102:4487–4492.
11. Marshall, J.D., K. Fearon, C. Abbate, S. Subramanian, P. Yee, J. Gregorio, R.L. Coffman, and G. Van Nest. 2003. Identification of a novel CpG DNA class and motif which optimally stimulate B cell and plasmacytoid dendritic cell functions. *J. Leukoc. Biol.* 73:781–792.
12. Hartmann, G., J. Battiany, H. Poeck, M. Wagner, M. Kerkmann, N. Lubenow, S. Rothenfusser, and S. Endres. 2003. Rational design of new CpG oligonucleotides that combine B cell activation with high IFN-α induction in plasmacytoid dendritic cells. *Eur. J. Immunol.* 33:1633–1641.
13. Honda, K., H. Yanai, H. Negishi, M. Asagiri, M. Sato, T. Mizutani, N. Shimada, Y. Ohba, A. Takaoka, N. Yoshida, and T. Taniguchi. 2005. IRF-7 is the master regulator of type-I interferon-dependent immune responses. *Nature.* 434:772–777.
14. Honda, K., Y. Ohba, H. Yanai, H. Negishi, T. Mizutani, A. Takaoka, C. Taya, and T. Taniguchi. 2005. Spatiotemporal regulation of MyD88-IRF-7 signalling for robust type-I interferon induction. *Nature.* 434:1035–1040.
15. Latz, E., A. Schoenemeyer, A. Visintin, K.A. Fitzgerald, B.G. Monks, C.F. Knetter, E. Lien, N.J. Nilsen, T. Espevik, and D.T. Golenbock. 2004. TLR9 signals after translocating from the ER to CpG DNA in the lysosome. *Nat. Immunol.* 5:190–198.
16. Gruenberg, J., and H. Stenmark. 2004. The biogenesis of multivesicular endosomes. *Nat. Rev. Mol. Cell Biol.* 5:317–323.
17. Perret, E., A. Lakkaraju, S. Deborde, R. Schreiner, and E. Rodriguez-Boulan. 2005. Evolving endosomes: how many varieties and why? *Curr. Opin. Cell Biol.* 17:423–434.
18. Marshall, J.D., D. Higgins, C. Abbate, P. Yee, G. Teshima, G. Ott, T. dela Cruz, D. Passmore, K.L. Fearon, S. Tuck, and G. Van Nest. 2004. Polymyxin B enhances ISS-mediated immune responses across multiple species. *Cell. Immunol.* 229:93–105.
19. Drummond, D.C., M. Zignani, and J. Leroux. 2000. Current status of pH-sensitive liposomes in drug delivery. *Prog. Lipid Res.* 39:409–460.
20. Maxfield, F.R., and T.E. McGraw. 2004. Endocytic recycling. *Nat. Rev. Mol. Cell Biol.* 5:121–132.
21. Lee, K.D., Y.K. Oh, D.A. Portnoy, and J.A. Swanson. 1996. Delivery of macromolecules into cytosol using liposomes containing hemolysin from *Listeria monocytogenes*. *J. Biol. Chem.* 271:7249–7252.
22. Mandal, M., and K.D. Lee. 2002. Listeriolysin O-liposome-mediated cytosolic delivery of macromolecule antigen in vivo: enhancement of antigen-specific cytotoxic T lymphocyte frequency, activity, and tumor protection. *Biochim. Biophys. Acta.* 1563:7–17.
23. Tabeta, K., K. Hoebe, E.M. Janssen, X. Du, P. Georgel, K. Crozat, S. Mudd, N. Mann, S. Sovath, J. Goode, et al. 2006. The Unc93b1 mutation 3d disrupts exogenous antigen presentation and signaling via Toll-like receptors 3, 7 and 9. *Nat. Immunol.* 7:156–164.
24. Trombetta, E.S., M. Ebersold, W. Garrett, M. Pypaert, and I. Mellman. 2003. Activation of lysosomal function during dendritic cell maturation. *Science.* 299:1400–1403.
25. Rutz, M., J. Metzger, T. Gellert, P. Luppa, G.B. Lipford, H. Wagner, and S. Bauer. 2004. Toll-like receptor 9 binds single-stranded CpG-DNA in a sequence- and pH-dependent manner. *Eur. J. Immunol.* 34:2541–2550.
26. Morilla, M.J., J. Montanari, F. Frank, E. Malchiodi, R. Corral, P. Petray, and E.L. Romero. 2005. Etanidazole in pH-sensitive liposomes: design, characterization and in vitro/in vivo anti-*Trypanosoma cruzi* activity. *J. Control. Release.* 103:599–607.
27. Huth, U.S., R. Schubert, and R. Peschka-Suss. 2006. Investigating the uptake and intracellular fate of pH-sensitive liposomes by flow cytometry and spectral bio-imaging. *J. Control. Release.* 110:490–504.
28. Miaczynska, M., L. Pelkmans, and M. Zerial. 2004. Not just a sink: endosomes in control of signal transduction. *Curr. Opin. Cell Biol.* 16:400–406.
29. Sieczkarski, S.B., and G.R. Whittaker. 2002. Dissecting virus entry via endocytosis. *J. Gen. Virol.* 83:1535–1545.
30. Smith, A.E., and A. Helenius. 2004. How viruses enter animal cells. *Science.* 304:237–242.
31. Sieczkarski, S.B., and G.R. Whittaker. 2003. Differential requirements of Rab5 and Rab7 for endocytosis of influenza and other enveloped viruses. *Traffic.* 4:333–343.
32. Vonderheit, A., and A. Helenius. 2005. Rab7 associates with early endosomes to mediate sorting and transport of Semliki forest virus to late endosomes. *PLoS Biol.* 3:e233.
33. Beignon, A.S., K. McKenna, M. Skoberne, O. Manches, I. Dasilva, D.G. Kavanagh, M. Larsson, R.J. Gorelick, J.D. Lifson, and N. Bhardwaj. 2005. Endocytosis of HIV-1 activates plasmacytoid dendritic cells via Toll-like receptor-viral RNA interactions. *J. Clin. Invest.* 115:3265–3275.
34. Yoneyama, H., K. Matsuno, E. Toda, T. Nishiwaki, N. Matsuo, A. Nakano, S. Narumi, B. Lu, C. Gerard, S. Ishikawa, and K. Matsushima. 2005. Plasmacytoid DCs help lymph node DCs to induce anti-HSV CTLs. *J. Exp. Med.* 202:425–435.
35. Marshall, J.D., E.M. Hessel, J. Gregorio, C. Abbate, P. Yee, M. Chu, G. Van Nest, R.L. Coffman, and K.L. Fearon. 2003. Novel chimeric immunomodulatory compounds containing short CpG oligodeoxyribonucleotides have differential activities in human cells. *Nucleic Acids Res.* 31:5122–5133.
36. Inman, J.K. 1975. Thymus-independent antigens: the preparation of covalent, hapten-ficoll conjugates. *J. Immunol.* 114:704–709.
37. Duramad, O., K.L. Fearon, B. Chang, J.H. Chan, J. Gregorio, R.L. Coffman, and F.J. Barrat. 2005. Inhibitors of TLR-9 act on multiple cell subsets in mouse and man in vitro and prevent death in vivo from systemic inflamation. *J. Immunol.* 174:5193–5200.
38. Monnard, P.A., T. Oberholzer, and P. Luisi. 1997. Entrapment of nucleic acids in liposomes. *Biochim. Biophys. Acta.* 1329:39–50.